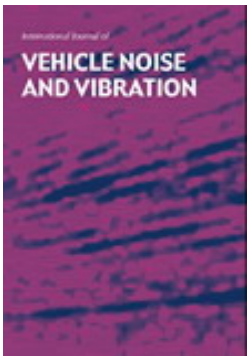

International Journal of Vehicle Noise and Vibration

ISSN online: 1479-148X - ISSN print: 1479-1471
https://www.inderscience.com/ijvnv

Research on the vibration isolation performance of low-frequency hydraulic engine mount

Zhihong Lin, Yunxiao Chen, Mingzhong Wu

DOI: 10.1504/IJVNV.2023.10055214

Article History:
Received: 07 August 2022
Accepted: 02 January 2023
Published online: 10 April 2023

Research on the vibration isolation performance of low-frequency hydraulic engine mount

Zhihong Lin*

School of Mechanical and Electrical Engineering,
Sanming University,
Sanming Fujian 365004, China
Email: lin123hongzhi@163.com
*Corresponding author

Yunxiao Chen and Mingzhong Wu

College of Mechanical Engineering and Automation,
HuaQiao University,
Xiamen, 361021, China
Email: chenyx@stu.hqu.edu.cn
Email: jdwmz62@hqu.edu.cn

Abstract: This paper aims to study the influence of decoupler membranes on the vibration isolation performance of hydraulic mount under low-frequency excitation. Firstly, the mathematical model of the hydraulic mount is constructed using the lumped parameters and the accuracy of the mathematical model is confirmed. Secondly, the influence of the dynamic characteristics and flow rate of the hydraulic mount under different excitation amplitudes and excitation frequencies is analysed. Finally, the hydraulic mount system of the 1/4 car model is built to analyse the effect of with or without decoupler membrane channels on the vibration isolation performance of the system from sinusoidal excitation, random road spectrum, and different engine speeds. The results of the study show that the decoupler membrane directly affects the hydraulic mount in low frequency vibration isolation performance.

Keywords: hydraulic mount; decoupler membrane; quarter car model; vibration isolation.

Reference to this paper should be made as follows: Lin, Z., Chen, Y. and Wu, M. (2023) 'Research on the vibration isolation performance of low-frequency hydraulic engine mount', *Int. J. Vehicle Noise and Vibration*, Vol. 19, Nos. 1/2, pp.78–97.

Biographical notes: Zhihong Lin is currently working at the School of Mechanical and Electrical Engineering, Sanming University, China. He graduated from the Huaqiao University with a PhD in Mechanical Engineering. He received his MS in Marine and Offshore Engineering from the Jimei University. His research interests include control, dynamics, and vehicle NVH.

Yunxiao Chen is a PhD candidate at the Huaqiao University. He obtained his MSc in the College of Computer Science of Huaqiao University. His current research project focuses on robotics control.

Mingzhong Wu holds a PhD from the College of Mechanical, Electrical and Automation, Huaqiao University, Xiamen, China. Currently, he works at Xiamen. His current research interests include vibration and control.

1 Introduction

The main sources of car vibration are the torsional and unbalanced inertial forces from low engine speed and high speed as well as road excitation (Truong and Ahn, 2010; Shangguan, 2009). The amplitude of the unbalanced inertia force of the engine and the torque fluctuation of combustion is less than 0.3 mm and the frequency is 25 Hz–250 Hz, which is called high frequency and small amplitude excitation; the amplitude of the excitation caused by the uneven surface of the road is greater than 0.3 mm or 0.5 mm and the frequency is 1 Hz–30 Hz, which is called low frequency and large amplitude excitation (Yu et al., 2001a, 2001b). Especially in harsh conditions offshore, the requirements for car vibration isolation are more stringent. So, a reasonable design of the mount can reduce the vibration brought by the engine and the road is very meaningful research. The engine stopping time at idle accounts for more than 1/3 of the car running time, and the deceleration phase accounts for more than half of the car running time (Hafidi et al., 2010). Therefore, engine mounts play a crucial role in noise and vibration comfort (Qatu et al., 2009; Qatu, 2012). Due to the strong frequency and amplitude dependence of the mounts themselves, passive hydraulic mounts that are higher than passive rubber mounts are proposed (Singh et al., 1992). Meanwhile, semi-active or active mounts have recently grown up to be a hot research topic (Deng et al., 2020; Yang et al., 2017; Lee, 2009). However, passive hydraulic mounts are still commonly used due to their simple design and low cost. At present, the inertial channel and decoupler membrane combination hydraulic mounts are relatively mature in both frequency domain and time domain characteristics.

Passive hydraulic mount structures are mainly inertia channel (or damping hole) and inertia channel decoupler membrane hydraulic mounts. A typical hydraulic mount consists of two fluid-filled chambers connected by a decoupler membrane and an inertial channel. The hydraulic mount of the inertia channel (or orifice) only gets small holes, spiral or annular inertia channels connected between the two chambers, where the inertia channel is a tube with a certain cross-sectional area and a certain length. The amount of fluid mass inside the tube is dependent on the cross-sectional area and length, and the inertia can be massively varied. When the mounts are excited, the mass of fluid flows back and forth inside the tube, in and out of the upper and lower chambers. Therefore, large damping characteristics at low frequencies can control the displacement of engine vibration (Marzbani et al., 2014). However, the high-frequency hardening phenomenon can occur, which degrades the vibration isolation effect. Inertia channel decoupler membrane hydraulic mount is to add decoupler membrane based on inertia channel hydraulic mount, to solve the problem of high-frequency hardening. Since the decoupler membrane is located inside the decoupler cage, when the mounts are excited by high-frequency small-amplitude values, the decoupler membrane simply oscillates, suspended between the top and bottom chambers of the decoupler cage. The resistance to flow through the decoupler membrane is much less than the resistance to flow through the inertial channel. Therefore, under high frequency and small amplitude excitation, the

fluid mainly enters the lower chamber through the decoupler membrane, which makes the mount exhibit low damping characteristics (Golnaraghi and Jazar, 2001).

Hydraulic mount modelling provides a clear understanding of the characteristics of the mounts and the analysis of vibration isolation performance. Singh et al. (1992) took the lead in linearising the hydraulic mounts and modelling them mathematically using set lumped parameters. And based on the mathematical model, the correctness of the model is experimentally verified at a frequency of 1 Hz–50 Hz. Followed by Singh et al. who developed linear and nonlinear models of hydraulic mounts being combined with theoretical analysis and experiments using a lumped parameter approach, and then dynamic characterisation and transient response analysis were performed (Kim and Singh, 1995; He and Singh, 2005, 2007; Lee and Singh, 2008). Geisberger et al. (2002) developed a complete mathematical model of the nonlinear hydraulic mount, which reveals the working process of the nonlinear decoupler membrane in the form of mathematical. Yoon and Singh (2010a, 2010b) proposed linear time-invariant, nonlinear and quasi-linear fluid and mechanical system models due to the background of the more difficult direct measurement of hydraulic mount transfer forces. And, the model is utilised to predict the transfer force of the hydraulic mounts under sinusoidal excitation conditions for a given measured (or calculated) motion and/or internal pressure. To improve the vibration isolation performance of the hydraulic mount. The controllable inertia channel cross-sectional area, the inertia channel length, and the flexibility of the upper chamber are adjusted. Foumani et al. (2002, 2003, 2004) proposed adjustable inertia channel length as well as a shape memory alloy type of semi-active hydraulic mount developed and sensitivity analysis of relevant parameters. Barszcz et al. (2012) added inertia channels to the existing inertia channel and decoupler membrane structure from experimental and analytical studies on the dynamic characteristics of hydraulic mounts when the number of inertia channels is greater than 2. Li et al. (2019) proposed an inertial channel optimisation method based on a linearise low-frequency model excluding the effect of decoupler membranes, considering multiple arrangements of inertial channel and hole combinations. Because of the specificity of the mount work, the engine frequency is 25 Hz–250 Hz, and the excitation frequency of the road is 0 Hz–30 Hz. Therefore, the current mathematical modelling of passive hydraulic mounts or semi-active hydraulic mounts is 0 Hz–30 Hz considering the inertial channel as the basis and the role of the decoupler membrane. Similarly, at 25 Hz–250 Hz it is considered that the decoupler membrane ignores the role of inertial channels. Although, mathematical modelling of hydraulic mounts according to different excitation amplitude and excitation frequencies has been verified experimentally. However, during the actual car driving, the engine and the road are input at the same time. Neglected in the mathematical modelling when the engine and road surface overlap each other. In summary, there are few reports on the interaction of decoupler membrane with inertial channels at different excitation frequencies and excitation amplitude. In particular, there are fewer studies on the dynamic characteristics and vibration isolation performance of hydraulic mounts at different excitation frequencies and excitation amplitude of decoupler membranes interacting with inertial channels.

For engine vibration isolation problems, this paper is to analyse the effect of whether to consider the decoupler membrane on the vibration isolation performance of the hydraulic mount system for the 1/4 car model. A hydraulic mount system for a 1/4 car model is built, where the hydraulic mount is referenced to the model proposed by

Geisberger et al. (2002). Built on the mathematical model the following points are analysed:

1 According to the mathematical model, the frequency domain characteristics of the hydraulic mount with large amplitude at low frequency and small amplitude at high frequency are analysed.

2 Analyse the effects of different excitation frequencies and different excitation amplitude on the flow and pressure of inertial channel and decoupler membrane.

3 Effect of random road excitation and engine excitation on hydraulic mount vibration isolation performance with and without decoupler membrane on class B road, class C road, idling conditions, and crossing speed bumps.

2 Hydraulic mount model

2.1 Hydraulic mount mathematical modelling

Figure 1 shows a schematic diagram of the hydraulic mount, where Figure 1(a) shows the structure of the hydraulic mount, and Figure 1(b) shows the lumped parameter model of the hydraulic mount. In practical cars, it usually consists of three to four mounts, one or two of which are hydraulic mounts. The top of the mounts are attached to the engine and the bottom is mounted on the chassis of the car. Engine mounts are supported by mainspring rubber elements providing a certain amount of stiffness and damping to support the weight of the static engine, denoted by K_r and B_r, respectively. Upper and lower chambers are filled with a mixture of antifreeze and water, and when the mount is externally excited the fluid will flow through the inertia channel and the decoupler disk channel when the narrow inertia channel provides a large fluid damping, where the flow rate through the inertia channel and decoupler membrane are denoted by Q_i and Q_d, respectively. When the fluid flows from the upper chamber to the lower chamber, the flexible rubber membrane plays the role of energy storage. C_1 and C_2 are the compliance of the upper and lower cavities, P_1 and P_2 are the pressures of the upper and lower chambers, and A_p is the equivalent upper chamber cross-sectional area. According to Figure 1(b), the mathematical equations (1)–(6) of the lumped parameters of the hydraulic mount can be solved.

$$P_1(t) - P_2(t) = I_i \dot{Q}_i(t) + R_i Q_i(t) + 1/2K\rho |\dot{x}_i| \dot{x}_i \tag{1}$$

$$P_1(t) - P_2(t) = I_d \dot{Q}_d(t) + R_d Q_d(t) \tag{2}$$

$$\dot{P}_1(t) = \frac{A_p}{C_1} \dot{x}_e(t) - \frac{Q_i(t) + Q_d(t)}{C_1} \tag{3}$$

$$\dot{P}_2(t) = \frac{Q_i(t) + Q_d(t)}{C_2} \tag{4}$$

$$I_i = \frac{\rho L}{A_i} \tag{5}$$

$$R_i = \frac{128\eta L}{\pi D_h^4} \tag{6}$$

where I_i and R_i are the inertia and fluid resistance of the fluid passing through the inertia channel, $\dot{x}_i$ is the average flow velocity of the fluid in the inertia channel, K is the local resistance coefficient of the fluid inlet and outlet of the inertia channel, I_d and R_d are the inertia and fluid resistance of the fluid passing through the decoupler membrane, ρ is the density of the fluid, L is the length of the flow channel, A_i is the cross-sectional area of the flow channel, and η is the viscosity of the fluid, and D_h is the equivalent 'hydraulic diameter' of the flow path. The first term on the right side of equations (1) and (2) is the pressure drop due to the inertia of the fluid flowing in the inertial channel and the decoupler membrane; the second term on the right side is the pressure drop due to the viscous damping of the fluid flowing in the inertial channel and the decoupler membrane. $1/2K\rho|\dot{x}_i|\dot{x}_i$ in equation (1) is the pressure drop from local flow losses at the inlet and outlet of the inertia channel fluid is taken into account.

Figure 1 Hydraulic mount, (a) structure diagram, (b) lumped parameter model (see online version for colours)

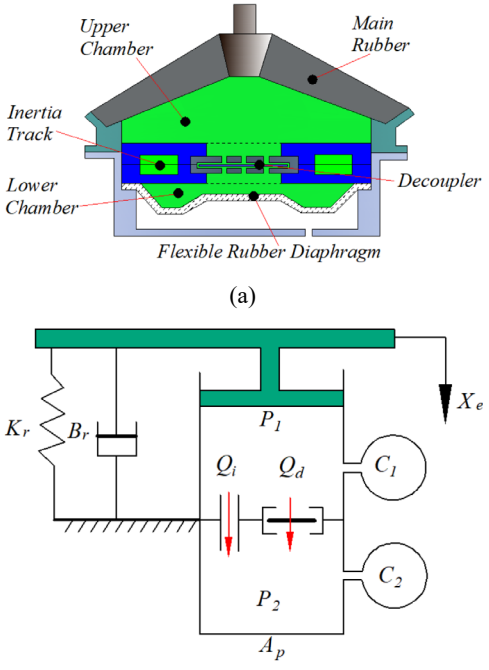

Since the decoupler membrane is highly nonlinear during the motion. In the paper, reference (Li et al., 2019) uses a nonlinear decoupler membrane resistance for modelling the switching mechanism of the decoupling membrane at different frequencies, and its expression is shown in equation (7).

$$R_d = R_{dd} + R_0 e^{(x_d/x_0)\arctan(Q_d/Q_0)} \tag{7}$$

where R_{dd} is the linear fluid resistance to flow through the decoupler membrane and $x_d = V_d / A_d$ is the position of the decoupler membrane. The flow volume for the decoupler is represented by $V_d = \int Q_d dt$, A_d is the area of the decoupler membrane, x_0 is the height of the decoupler cage, and Q_0 is used to produce a clear switching response, R_0 is the nonlinear resistance constant in the decoupler.

Then according to equations (1)–(7) the transmission force from the mount to the chassis can be obtained as:

$$F_T = B_r \dot{x}_e(t) + K_r x_e(t) + \left(A_p - A_{dfnc}\right)\left(P_1(t) - P_2(t)\right) + A_p P_2(t) + A_d R_d Q_d(t) \tag{8}$$

In equation (8), A_{dfnc} is used to express the effective area change of the decoupler membrane at different excitation amplitudes, using the arctangent function to the pressure difference and decoupler membrane displacement as an expression. Where A_{dfnc} is solved with reference to the literature [16] as shown in equation (9).

$$A_{dfnc} = 0.5A_d - \frac{A_d}{\pi}\arctan\left(\frac{\frac{2}{\pi}x_d \arctan\left[\left(P_1 - P_2\right)\Big/ P_0\right] - x_{dmax}}{x_1}\right) \tag{9}$$

where P_0 and x_1 are constants used to normalise the function and control the switching function, x_{dmax} is half of the height of the decoupling cage.

2.2 Hydraulic mount mathematical model validation and analysis

A fast Fourier transform of equation (8) obtains the expression for the complex stiffness of the hydraulic mount.

$$K_h(\omega) = \frac{F_T}{x_e}(\omega) \tag{10}$$

According to equation (10), the complex stiffness $K_h(\omega)$ can be expressed by the stored dynamic stiffness K' and the lost dynamic stiffness K'', as shown in equation (11).

$$K_h = K' + jK'' \tag{11}$$

Therefore, the expressions for the dynamic stiffness K_d and the loss angle φ of the hydraulic mounts are:

$$K_d = \sqrt{K'^2 + K''^2},\ \varphi = \tan^{-1}\left(\frac{K''}{K'}\right) \tag{12}$$

To verify the correctness of the model is compared with the experimental data of reference 16], as shown in Figure 2, the excitation amplitude X_e = 2.0 mm, excitation frequency f = 0 Hz~40 Hz. Where the red solid line is the lumped parameter model derived in this paper and the blue dashed line is the experimental data from Geisberger et al. (2002). From Figure 2, we can obtain that the error between the two is very small, which can verify the correctness of the lumped parameter model.

Figure 2 Frequency domain characteristics of hydraulic mount, (a) dynamic stiffness, (b) loss angle (see online version for colours)

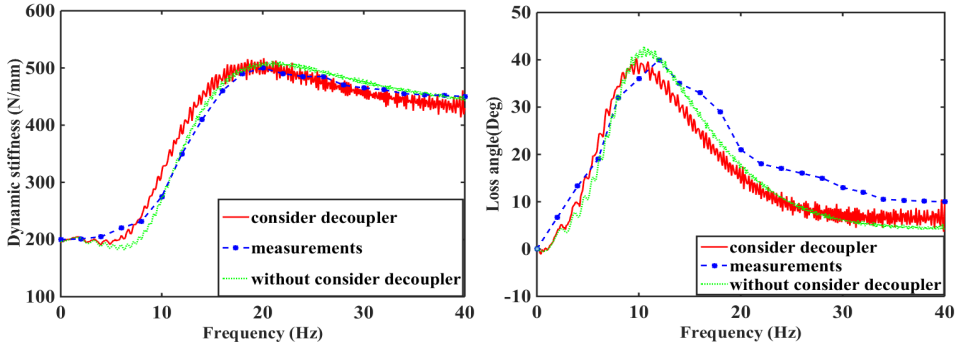

(a) (b)

Table 1 Parameters values used in the analysis

Parameter	*Symbol*	*Value*
Effective piston area	A_p	$2.5 \times 10^{-3}\text{m}^2$
Upper chamber stiffness	K_r	$2.0 \times 10^{5}\text{N/m}$
Upper chamber damping	B_r	100/N·sm
Upper chamber compliance	C_1	$3.5 \times 10^{-11}\text{m}^5/\text{N}$
Lower chamber compliance	C_2	$2.6 \times 10^{-9}\text{m}^5/\text{N}$
Fluid inertia in decoupler	I_d	$7.5 \times 10^{4}\text{kg/m}^4$
Inertia channel length	L	212 mm
Density of liquid	ρ	$2.66 \times 10^{3}\text{kg/m}^3$
Viscosity of liquid	η	0.06pa·s
Pressure normalised constant	P_0	$10\ \text{N/m}^2$
Flow normalised constant	Q_0	$1.0 \times 10^{-14}\text{m}^3/\text{s}$
Linear fluid resistance in decoupler	R_d	$1.17 \times 10^{7}\text{kg/(s·m}^4\text{)}$
Nonlinear resistance constant in decoupler	R_0	$1.0 \times 10^{-4}\text{kg/(s·m}^4\text{)}$
Half decoupler cage height	X_{dmax}	$5.3 \times 10^{-4}\text{m}$
Decoupler position control constant	X_0	$2.62 \times 10^{-5}\text{m}$
Decoupler switching function shape control constant	X_1	$1.0 \times 10^{-9}\text{m}$

Refer to Table 1, the frequency response characteristics (dynamic stiffness and loss angle) of the hydraulic mount were calculated numerically under the low-frequency 0 Hz–30 Hz excitation amplitude, X_e = 3.0 mm, as shown in Figure 3(a). Figure 3(a) shows that the dynamic stiffness and loss angle of the hydraulic mounts have a strong frequency dependence. The initial values of dynamic stiffness and loss angle of hydraulic mount start from 200 N/m and 0(Deg) respectively and then increase with the increase of frequency, then reach the natural frequency and peak frequency of dynamic stiffness and loss angle, and then decrease slowly with the increase of excitation amplitude x_e. Similarly, numerical calculations were performed for high frequency 0–250 Hz with excitation amplitudes of X_e = 0.05 mm, respectively, as shown in Figure 3(b). The dynamic characteristics of the hydraulic mount under high-frequency excitation are similar to those of the low-frequency with frequency dependence.

Figure 3 Frequency domain characteristics of hydraulic mount, (a) X_e = 3.0 mm, (b) X_e = 0.05 mm (see online version for colours)

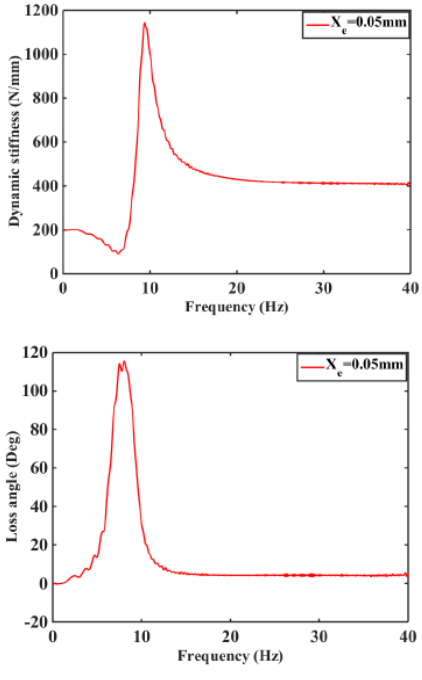

(a)

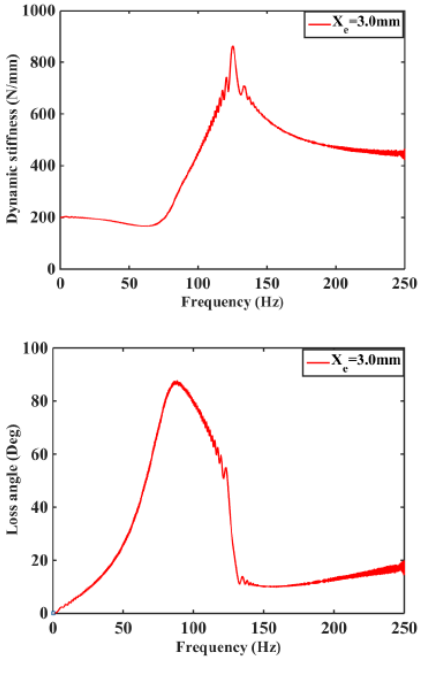

(b)

Figure 4 Inertial channel and decoupler membrane flow, (a) f = 5 Hz, 3.0 mm, (b) f = 100 Hz, 0.05 mm (see online version for colours)

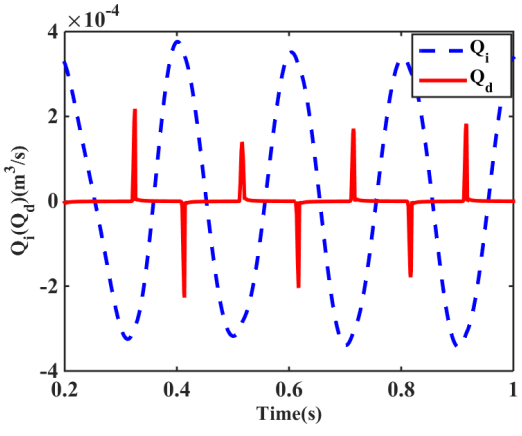

(a)

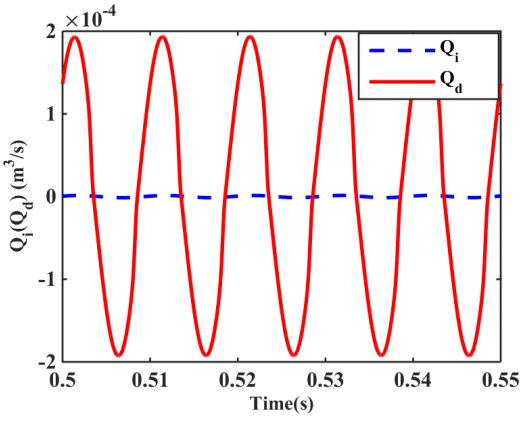

(b)

To analyse the role between the decoupler membrane and the inertial channel, the steady-state time-domain responses of Q_i and Q_d are calculated at 5 Hz, 3.0 mm and 100 Hz, 0.05 mm, respectively, as shown in Figure 4. It can be seen that at f = 5 Hz, the effective flow through the decoupler membrane is negligible compared to the effective flow through the inertial channel. At f = 100 Hz, the effective flow through the decoupler membrane is greater than the effective flow through the inertial channel. It can be seen that the inertia channel plays a decisive role in the hydraulic mount at large amplitude at low frequency, while the decoupler membrane makes the main contribution to the hydraulic mount vibration isolation at small amplitude at high frequency. However, when the road excitation and engine excitation overlap each other part, the inertial channel and the decoupler membrane work at the same time, and the inertial channel and the decoupler membrane cannot be separated in to high and low frequencies directly. The inertial channel flow at the black oval of the paper in Figure 5(a) is greater than the flow during the commutation of the decoupler membrane motion, and similarly, the upper chamber pressure in Figure 5(b) has a slight jump at the black oval, which are due to the

effect of the interaction between the inertial channel and the decoupler membrane. When the decoupler membrane is moving from one direction to another, the flow rate reaches the maximum before the limit position of the decoupler membrane, which is higher than the flow rate of the inertia channel at this time.

Figure 5 Flow rate of inertial channel and decoupler membrane at 25 Hz, 0.5 mm, (a) inertial channel and decoupler membrane flow, (b) upper chamber pressure (see online version for colours)

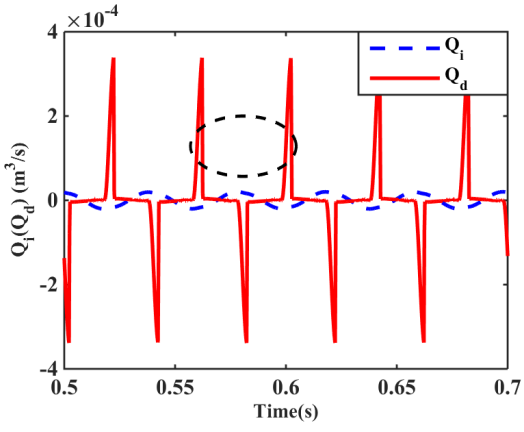

(a)

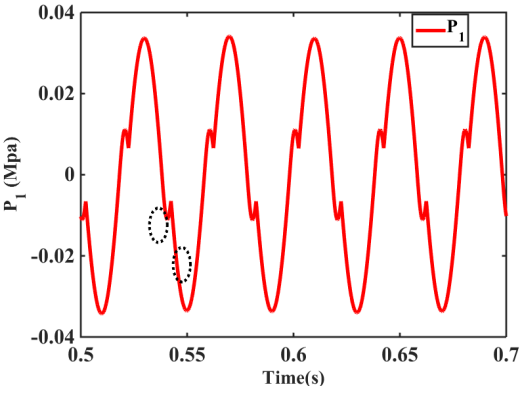

(b)

Figure 6 numerically calculates the effect of the inertial channel and decoupler membrane on the mount when the hydraulic mount is subjected to a step response of 0.05 mm and 1.0 mm. Figure 6(b) shows that the flow in the inertial channel is almost negligible at an amplitude of 0.05 mm. At this time, the attenuation of the transfer force is mainly caused by the damping generated by the liquid flowing through the decoupler membrane channel as shown in Figure 6(a). When the step response of amplitude is 1.0 mm, the inertial channel and the decoupler membrane channel act simultaneously, as shown by the red solid and red dashed lines in Figure 6(b). At this time, the transfer force decay is a result of the combined effect of fluid flow through the inertial channel and the decoupler membrane channel. In particular, as the pressure in the upper chamber is

greater than the pressure in the lower chamber, the decoupler membrane starts to move downward. At this point, the decoupler membrane channel is opened, and the flow through the decoupler membrane channel tries to balance the pressure difference between the upper chamber and the lower chamber and prevents the increase in the upper chamber. At the same time, although the decoupler membrane is moving downward, the inertia channel causes the flow rate $Q_i > 0$ due to the liquid inertia effect, so the flow rate through the inertia channel is reversed from the flow rate through the decoupler membrane channel, in Figure 6(b).

Figure 6 Effect of step response on hydraulic mount, (a) transfer force, (b) inertia channel and decoupler membrane flow (see online version for colours)

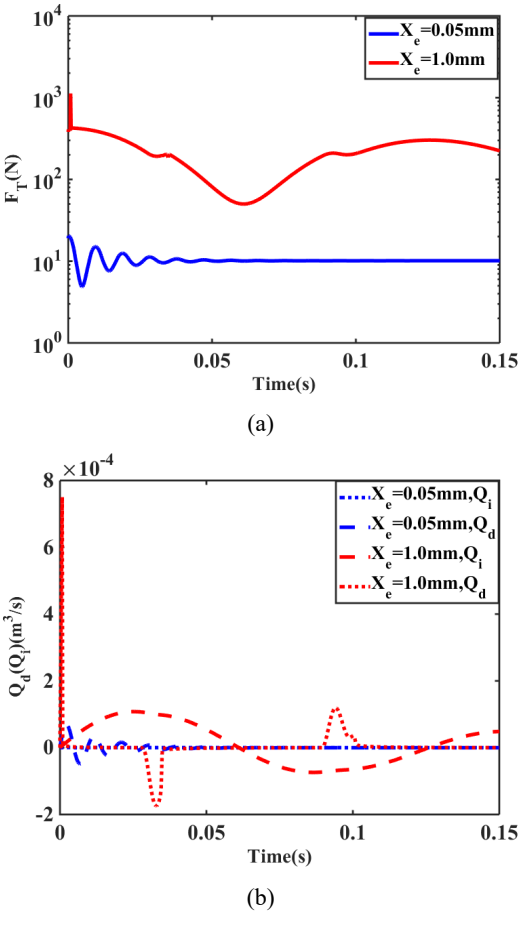

The above is an analysis of the effect of a single hydraulic mount element with and without decoupler channels on the mount characteristics under the action of low frequency and large amplitude excitation from the frequency and time domains. However, in order to reveal more clearly the effect of hydraulic mounts with and without decoupler membrane channels on the vibration isolation performance of the system under low frequency large amplitude excitation. Therefore, an in-depth study of the suspension

system from the perspective of considering road excitation and engine excitation is needed.

3 Effect of vibration isolation performance of hydraulic suspension system of 1/4 car model

3.1 Mathematical model of hydraulic mount system for 1/4 car model

To truly reflect the effect of the presence or absence of decoupler membrane on the vibration isolation performance of the hydraulic mount system, a hydraulic mount system for the 1/4 car model is built, as shown in Figure 7. The system includes hydraulic mount, suspension, and tyres, where K_u and B_u denote the suspension stiffness and damping, and K_t is the tyre stiffness. And the system excitation sources include: engine excitation $F_{exc}(t)$ and road input $h(t)$, $x_e(t)$, $y_c(t)$ and $z_w(t)$ denote the engine displacement, car frame displacement and under suspension unspring displacement, respectively. The mathematical model of the hydraulic mount system for the 1/4 car model is shown in expression (13), and the specific parameters of the system are shown in Table 2.

Figure 7 Hydraulic mount system for 1/4 car model (see online version for colours)

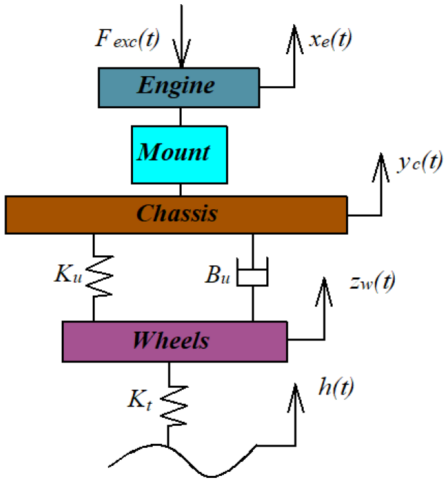

$$\begin{cases} M_e\ddot{x}_e + K_r\left(x_e - y_c\right) + B_r\left(\dot{x}_e - \dot{y}_c\right) + F = F_{exc} \\ M_b\ddot{y}_c - K_r\left(x_e - y_c\right) - B_r\left(\dot{x}_e - \dot{y}_c\right) + K_u\left(y_c - z_w\right) + B_u\left(\dot{y}_c - \dot{z}_w\right) - F = 0 \\ M_w\ddot{z}_w - K_u\left(y_c - z_w\right) - B_u\left(y_c - \dot{z}_w\right) + K_t\left(z_w - h\right) = 0 \end{cases} \tag{13}$$

where F of equation (13) is the damping force generated by the hydraulic mount.

To evaluate the vibration isolation of an engine mount, transmissibility is usually used. Transmissibility is the ratio of the active side vibration magnitude to the passive side vibration magnitude. At present, the main measures of engine mount transmissibility are engine and car frame vibration acceleration transmissibility and relative engine and car frame displacement transmissibility. The expressions for solving the acceleration transmissibility and relative displacement transmissibility are shown below.

$$T_{ap} = \frac{a_a}{a_p} \tag{14}$$

$$T_{x-y} = \left| \frac{x_e - y_c}{y_c} \right| \tag{15}$$

In this equation, T_{ap} is the acceleration transmissibility and T_{x-y} is the relative displacement transmissibility; and a_a is the engine vibration acceleration, a_p is the car frame vibration acceleration, x_e is the engine vibration displacement, and y_c is the car frame vibration displacement.

Table 2 Relevant parameters of the hydraulic mount system for 1/4 car model

Symbol	*Unit*	*Value*
M_e	kg	168
M_b	kg	890
M_w	kg	40
K_u	N/m	2.39×10^4
B_u	N·s/m	1,600
K_t	N/m	2.0×10^5

3.2 Introduction to engine excitation and road excitation

The road input model plays an important role in the car dynamics analysis and can reflect more realistically the effect of external excitation on the decoupler membrane and inertia channel. In this section, ISO I. 8608 (2016) is used to propose the classification of longitudinal random road surface unevenness based on power spectral density (PSD), and the time-frequency spectral density of road surface unevenness can be obtained whose solution expression is shown in equation (16).

$$\dot{h}(t) = -2\pi f_0 h(t) + 2\pi\sqrt{G_q(n_0)v}\omega(t) \tag{16}$$

In equation (16), f_0 is a constant, generally taken as 0.01 Hz; n_0 is the reference spatial frequency, n_0 = 0.1 m^{-1}; $G_q(n)$ is the value of the pavement spectrum at the reference spatial frequency, generally referred to as the unevenness value of the pavement, with unit of m^2/m^{-1}. $\omega(t)$ is the random white noise and v is the speed of the car. For class A road surface $G_q(n_0) = 16 \times 10^{-6}$ m^2/m^{-1}, class B road surface $G_q(n_0) = 64 \times 10^{-6}$ m^2/m^{-1}, class C road surface $G_q(n_0) = 256 \times 10^{-6}$ m^2/m^{-1}.

The subject of this study is the most common inline four-cylinder engine. Based on this type of engine it is known that the excitation consists mainly of even-order gas torque fluctuations, 2nd-order mass forces in the vertical direction, and mass torque around the X and Y directions. Therefore, the generalised excitation force of this four-cylinder engine is reflected in equation (17).

$$\{F_{exc}(t)\} = \{0 \quad F_y \quad F_z \quad M_x \quad M_y \quad 0\} \tag{17}$$

F_y is the force in the y-direction, F_z is the force in the z-direction, M_x is the torque around the x-direction, and M_y is the torque around the y-direction. Solve the following expressions.

$$\begin{cases} F_y = \sin\psi \cdot 4mr\lambda\omega^2 \cos 2\omega t \\ F_z = \cos\psi \cdot 4mr\lambda\omega^2 \cos 2\omega t \\ M_x \approx M_{e0}(1+1.3\sin 2\omega t) \\ M_y = F_z \cdot A \end{cases} \tag{18}$$

ψ is the tilt angle of the engine arrangement; m is the mass of the piston part; r is the radius of rotation of the crank; λ is the ratio of the crank radius to the length of the connecting rod, usually 0.25 to 0.33; ω is the angular velocity of the crankshaft of a four-cylinder engine; A is the horizontal distance from the centreline of the engine's second and third cylinders to the centre of mass of the powertrain. The relevant parameters of the engine are detailed in Table 3.

Table 3 Relevant parameters of the four-cylinder engine

Symbol	*Unit*	*Value*
M	kg	1.3
r	mm	45
L	mm	146
Λ	-	0.3028
A	mm	43.5

3.3 Vibration isolation effect of mount system with and without decoupler membrane under different road excitation and engine excitation

3.3.1 B/C class road-engine 2,000 r/min with or without decoupler membrane mount vibration isolation effect

According to the hydraulic mount system of the 1/4 car model built above, the B/C class road and engine 2,000 r/min with and without decoupler membrane channel engine transmissibility to vehicle frame acceleration transmissibility and engine and vehicle frame relative displacement transmissibility can be obtained. The results are shown in Figures 8 and 9.

Table 4 B-class road engine 2,000r/min mount vibration isolation effect comparison

Hydraulic mount	T_R *(1 Hz–30 Hz)*	T_R *(1 Hz–50 Hz)*	T_R *(25 Hz–50 Hz)*	T_a *(1 Hz–30 Hz)*	T_a *(1 Hz–50 Hz)*	T_a *(25 Hz–50 Hz)*
	RMS	*RMS*	*RMS*	*RMS*	*RMS*	*RMS*
Inertia channel	1.0943	0.8593	0.2104	0.6670	0.5176	0.0547
Decoupler channel	0.7354	0.5853	0.2033	4.2206	3.2741	0.2900

Figure 8 Acceleration transmissibility and displacement transmissibility of class B road mount system, (a) acceleration transmissibility, (b) relative displacement transmissibility (see online version for colours)

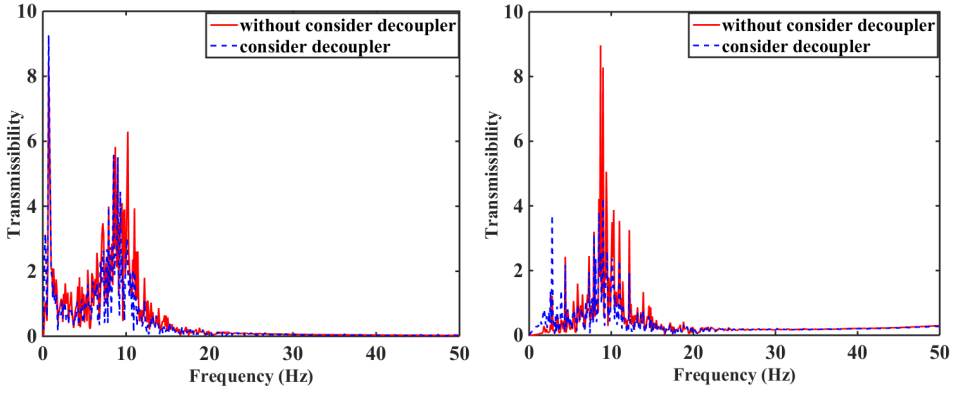

Figure 9 Acceleration transmissibility and displacement transmissibility of class C road mount system, (a) acceleration transmissibility, (b) relative displacement transmissibility (see online version for colours)

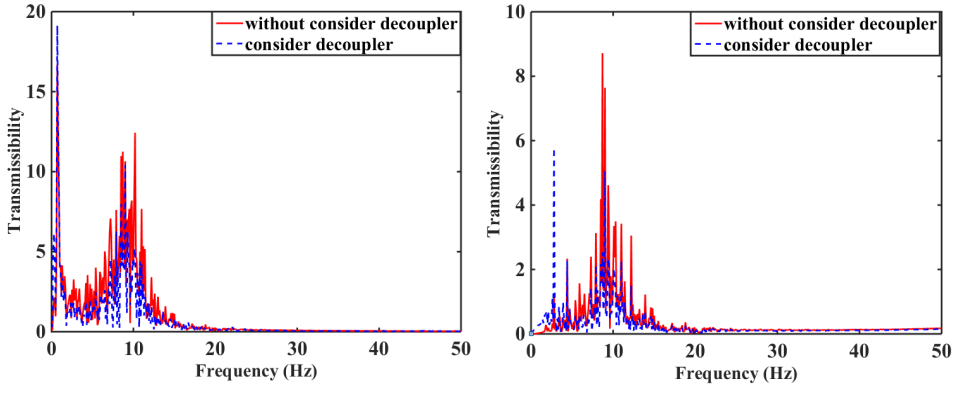

Table 5 C-class road engine 2,000r/min mount vibration isolation effect comparison

Hydraulic mount	T_R *(1 Hz–30 Hz)*	T_R *(1 Hz–50 Hz)*	T_R *(25 Hz–50 Hz)*	T_a *(1 Hz–30 Hz)*	T_a *(1 Hz–50 Hz)*	T_a *(25 Hz–50 Hz)*
	RMS	*RMS*	*RMS*	*RMS*	*RMS*	*RMS*
Inertia channel	1.0426	0.8127	0.1329	0.7741	0.6020	0.1061
Decoupler channel	0.6966	0.5449	0.1125	12.8436	9.9587	0.5699

In order to visually compare the vibration isolation effect with and without decoupled membrane channel mount system, the RMS values of the acceleration transmissibility transmitted from the engine to the vehicle frame and the relative displacement

transmissibility between the engine and the vehicle frame at 1 Hz–30 Hz, 1 Hz–50 Hz and 25 Hz–50 Hz are calculated respectively in Table 4 and Table 5, where T_R indicates relative displacement transmissibility, T_a indicates acceleration transmissibility.

As can be seen from Figure 8 and Table 4, the relative displacement transmissibility T_R of the hydraulic mount with decoupler membrane channel at excitation frequency 1 Hz–30 Hz, 1 Hz–50 Hz, and 25 Hz–50 Hz is 32.80%, 31.89%, and 3.37% lower than the RMS of the hydraulic mount with the inertial channel when the engine is driven at 2,000 r/min and at 20 m/s on class B roads, respectively. However, the acceleration transmissibility T_a increased by 84.20%, 84.19%, and 81.14%, respectively; over the RMS of the inertial channel hydraulic mount. Similarly, the vibration isolation performance of the hydraulic mount system with and without a decoupler membrane channel can be calculated in Figure 9 and Table 5. When the engine is driven at 2,000 r/min and at 20 m/s on a class C road, the relative displacement transmissibility T_R of the hydraulic mount with decoupler membrane channel at excitation frequency 1 Hz–30 Hz, 1 Hz–50 Hz, and 25 Hz–50 Hz is 33.19%, 32.95%, and 15.35% lower than the RMS of the hydraulic mount with the inertial channel, respectively. However, the acceleration transmissibility T_a increased by 93.97%, 93.96%, and 46.38%, respectively; over the RMS of the inertial channel hydraulic mount. From the above analysis, it is clear that the hydraulic mount with decoupler membrane channels exhibits greater damping at low-frequency excitation. Therefore, the relative displacement isolation effect of the hydraulic mount with a decoupler membrane channel at low frequency is better than that of the hydraulic mount with an inertia channel. At the same time, the acceleration isolation is worse than the inertia channel hydraulic mount. The reason for the difference in vibration isolation performance is that the decoupler membrane channel also has flowed through it at low-frequency large-amplitude excitation, causing the hydraulic mounts to exhibit greater damping.

3.3.2 Engine idle speed 600 r/min with or without decoupler membrane mount vibration isolation effect

Engine stopping time at idle accounts for more than 1/3 of the car's running time, and the deceleration phase accounts for more than half of the car's running time (Hafidi et al., 2010). Therefore, this subsection will take the engine idling condition as the starting point to numerically calculate and analyse whether to consider the decoupler membrane channel when the engine transfer to the car frame acceleration transmissibility and the engine and car relative displacement transmissibility effects. The simulation results are shown in Figure 10.

Table 6 Comparison of engine idle speed 600r/min mount vibration isolation effect

Hydraulic mount	T_R *(1 Hz–30 Hz)*	T_R *(1 Hz–50 Hz)*	T_R *(25 Hz–50 Hz)*	T_a *(1 Hz–30 Hz)*	T_a *(1 Hz–50 Hz)*	T_a *(25 Hz–50 Hz)*
	RMS	*RMS*	*RMS*	*RMS*	*RMS*	*RMS*
Inertia channel	14.3475	19.7979	25.1705	0.2004	0.1953	0.1873
Decoupler channel	10.9265	12.2933	14.0177	1.0443	1.0298	1.0093

Hydraulic mount system with and without a decoupler membrane channel. When the engine idles at 600 r/min, the relative displacement transmissibility T_R of the hydraulic

mount with decoupler membrane channel at excitation frequency 1 Hz–30 Hz, 1 Hz–50 Hz, and 25 Hz–50 Hz is 23.84%, 37.91%, and 44.31% lower than the RMS of the hydraulic mount with the inertial channel, respectively. However, the acceleration transmissibility T_a increased by 80.81%, 81.04%, and 81.44%, respectively; over the RMS of the inertial channel hydraulic mount. From the above analysis, it is clear that the hydraulic mount with decoupler membrane channel at engine idle speed exhibit greater damping. Therefore, the RMS value of the relative displacement isolation rate of the hydraulic mount with a decoupler membrane channel is smaller than that of the inertial channel hydraulic mount, while the RMS value of the acceleration is larger than that of the inertial channel hydraulic mount.

Figure 10 Acceleration transmissibility and relative displacement transmissibility of engine and car frame at idle speed, (a) acceleration transmissibility, (b) relative displacement transmissibility (see online version for colours)

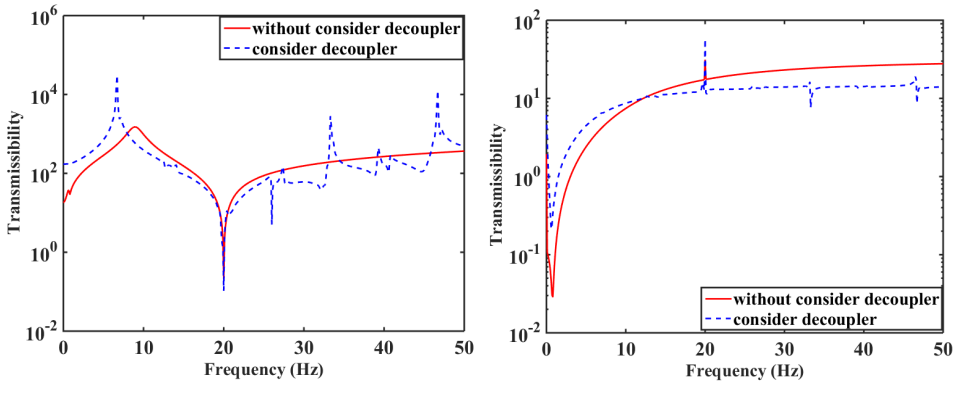

(a) (b)

3.3.3 *Over the speed bump with or without decoupler film mount vibration isolation effect*

When a car is on the road, there will inevitably be speed bumps. Numerical calculation and analysis of the engine transfer to the vehicle body acceleration transmissibility and engine and body relative displacement transmissibility changes for a car driving on a class A road engine 2,000 r/min at v = 2 m/s through a trapezoidal speed belt mount system with a height of 0.03 m. The simulation results are shown in Figure 11.

Table 7 Class A road-engine 2,000 r/min over speed bump mount vibration isolation effect comparison

Hydraulic mount	T_R *(1 Hz–30 Hz)*	T_R *(1 Hz–50 Hz)*	T_R *(25 Hz–50 Hz)*	T_a *(1 Hz–30 Hz)*	T_a *(1 Hz–50 Hz)*	T_a *(25 Hz–50 Hz)*
	RMS	*RMS*	*RMS*	*RMS*	*RMS*	*RMS*
Inertia channel	1.7236	1.3498	0.2900	0.5059	0.3924	0.0317
Decoupler channel	1.0388	0.8264	0.2787	5.4543	4.2283	0.1664

Figure 11 Class A road surface-engine 2,000 r/min over speed bump suspension system vibration isolation effect, (a) acceleration transmissibility, (b) relative displacement transmissibility (see online version for colours)

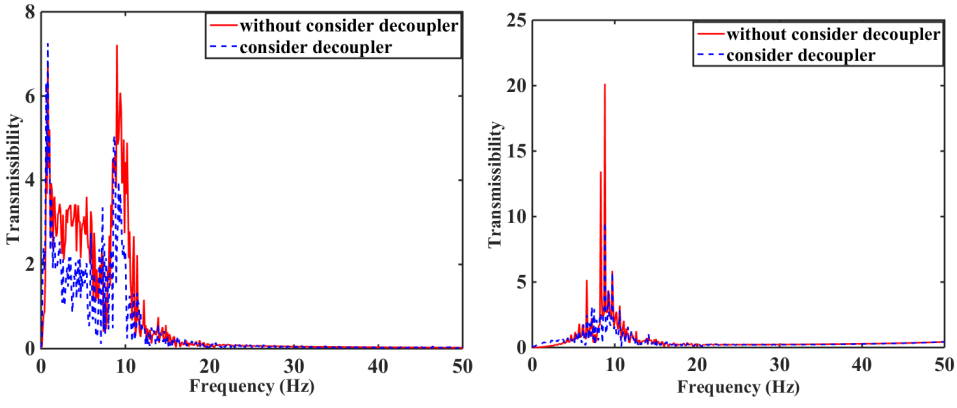

(a) (b)

As shown in Figure 11 and Table 7, the relative displacement transmissibility T_R of the hydraulic mount with decoupled membrane channel at excitation frequency 1 Hz–30 Hz, 1 Hz–50 Hz, and 25 Hz–50 Hz is 39.73%, 38.78%, and 3.90% lower than the RMS of the hydraulic mount with the inertial channel when the car is driven at 2 m/s over a speed bump on a class A roadway, respectively. However, the acceleration transmissibility T_a increased by 90.72%, 90.72%, and 80.95%, respectively; over the RMS of the inertial channel hydraulic mount. It can be seen that the relative displacement transmissibility of hydraulic mount with decoupler membrane channel under large amplitude excitation is better than that of inertial channel hydraulic mount. At the same time, the acceleration transmissibility of the hydraulic mount with a decoupler membrane channel under large amplitude excitation is worse than that of the inertial channel hydraulic mount.

4 Conclusions

The main contribution of the paper is to analyse the vibration isolation performance of hydraulic mounts with and without decoupler membrane channels under low-frequency large-amplitude excitation conditions and to analyse whether the effect of decoupler membrane channels needs to be taken into account when modelling the decoupler membrane hydraulic mount at low-frequency large amplitude. At present, the flow of the decoupler membrane channel is generally considered to be 0 when the decoupler membrane hydraulic mount is subjected to low frequency and large amplitude excitation, while there is a flow through the decoupler membrane channel. Therefore, it is necessary to consider the influence of the decoupler channel when analysing the dynamic characteristics of the decoupler membrane hydraulic mount under low-frequency large-amplitude excitation.

Firstly, the nonlinear model of hydraulic mount was established by referring to the model of hydraulic mount proposed by Geisberger et al. (2002), and the nonlinear model of hydraulic mount was established by using the lumped parameter method to verify the correctness of the model. Secondly, the dynamic stiffness and loss angle variations of the

high and low frequency decoupled membrane hydraulic mounts are analysed as well as the variations of the inertial channel and decoupled membrane channel flow from the time domain perspective with different excitation frequency and amplitude values. Meanwhile, the step response is calculated numerically at 0.1 mm and 1.0 mm as the amplitude to analyse the results of the interaction between the inertia channel and the decoupler membrane channel. Finally, a 1/4 car model was built to analyse the effect of vibration isolation with and without decoupler membrane channel on B/C class road-engine 2,000 r/min, engine idle 600 r/min, and over speed bumps with and without decoupler membrane mount. The results of the study show that the decoupler membrane channel has flow passing through it at a low frequency with large amplitude excitation. Therefore, the effect of the decoupler membrane channel action needs to be considered when modelling the hydraulic mount for the decoupler membrane, because in the low-frequency decoupler membrane channel there is fluid passing through making the suspension exhibit greater damping in favour of low-frequency displacement isolation.

References

Barszcz, B., Dreyer, J.T. and Singh, R. (2012) 'Experimental study of hydraulic engine mounts using multiple inertia tracks and orifices: narrow and broad band tuning concepts', *J. Sound Vib.*, Vol. 331, No. 24, pp.5209–5223.

Deng, Z., Yang, Q. and Yang, X. (2020) 'Optimal design and experimental evaluation of magneto-rheological mount applied to start/stop mode of car powertrain', *J. Intel. Mat. Syst. Str.*, Vol. 31, No. 8, pp.1126–1137.

Foumani, M.S., Khajepour, A. and Durali, M. (2002) 'Application of shape memory alloys to a new adaptive hydraulic mount', *International Body Engineering Conference & Exhibition and Automotive & Transportation Technology Congress*.

Foumani, M.S., Khajepour, A. and Durali, M. (2003) 'Application of sensitivity analysis to the development of high performance adaptive hydraulic engine mounts', *Car. Syst. Dyn.*, Vol. 39, No. 4, pp.257–278.

Foumani, M.S., Khajepour, A. and Durali, M. (2004) 'A new high-performance adaptive engine mount', *J. Vib. Control.*, Vol. 10, No. 1, pp.39–54.

Geisberger, A., Khajepour, A. and Golnaraghi, F. (2002) 'Non-linear modelling of hydraulic mounts: theory and experiment', *J. Vib. Control.*, Vol. 249, No. 2, pp.371–397.

Golnaraghi, M.F. and Jazar, G.N. (2001) 'Development and analysis of a simplified nonlinear model of a hydraulic engine mount', *J. Vib. Control.*, Vol. 7, No. 4, pp.495–526.

Hafidi, A.E., Martin, B., Loredo, A. and Jego, E. (2010) 'Vibration reduction on city buses: determination of optimal position of engine mounts, *Mech. Syst. Signal. Pr.*, Vol. 24, No. 7, pp.2198–2209.

He, S. and Singh, R. (2007) 'Approximate step response of a nonlinear hydraulic mount using a simplified linear model', *J. Vib. Control.*, Vol. 299, No. 3, pp.656–663.

He, S. and Singh, R. (2005) 'Estimation of amplitude and frequency dependent parameters of hydraulic engine mount given limited dynamic stiffness measurements', *Noise. Control. Eng. J.*, Vol. 53 No. 6, pp.271–285(15).

ISO I. 8608 (2016) *Mechanical Vibration-Road Surface Profiles-Reporting of Measured Data*, BSI Standards Publication, London, UK.

Kim, G. and Singh, R. (1995) 'A study of passive and adaptive hydraulic engine mount systems with emphasis on non-linear characteristics', *J. Sound Vib.*, Vol. 179, No. 3, pp.427–453.

Lee, B.H. (2009) 'Model based feed-forward control of electromagnetic type active control engine-mount system', *J. Sound Vib.*, Vol. 323, Nos. 3–5, pp.574–593.

Lee, J.H. and Singh, R. (2008) 'Nonlinear frequency responses of quarter car models with amplitude-sensitive engine mounts', *J. Vib. Control.*, Vol. 313, Nos. 3–5, pp.784–805.

Li, Y., Jiang, J.Z. and Neild, SA. (2019) 'Optimal fluid passageway design methodology for hydraulic engine mounts considering both low and high frequency performances', *J. Vib. Control.*, Vol. 25, Nos. 21–22, pp.2749–2757.

Marzbani, H., Jazar, R.N. and Fard, M. (2014) 'Hydraulic engine mounts: a survey', *J. Vib. Control.*, Vol. 20, No. 10, pp.1439–1463.

Qatu, M.S., Abdelhamid, M.K., Pang, J. et al. (2009) 'Overview of automotive noise and vibration', *International Journal of Vehicle Noise and Vibration*, Vol. 5, No. 1, pp.1–35.

Qatu, M.S. (2012) 'Recent research on vehicle noise and vibration', *International Journal of Vehicle Noise and Vibration*, Vol. 8, No. 4, pp.289–301.

Shangguan, W.B. (2009) 'Engine mounts and powertrain mounting systems: a review', *Int. J. Car. Des*., Vol. 49, No. 4, pp.237–258.

Singh, R., Kim, G. and Ravindra, P.V. (1992) 'Linear analysis of automotive hydro-mechanical mount with emphasis on decoupler characteristics, *J. Sound Vib.*, Vol. 158, No. 2, pp.219–243.

Truong, T.Q. and Ahn, K.K. (2010) 'A new type of semi-active hydraulic engine mount using controllable area of inertia track', *J. Sound Vib.*, Vol. 329, No. 3, pp.247–260.

Yang, S.Y., Han, C., Shin, S.U. and Choi, S.B (2017) 'Design and evaluation of a semi-active magneto-rheological mount for a wheel loader cabin', *Actuators*, Vol. 6, No. 2, p.16.

Yoon, J.Y. and Singh, R. (2010a) 'Indirect measurement of dynamic force transmitted by a nonlinear hydraulic mount under sinusoidal excitation with focus on super-harmonics', *J. Vib. Control.*, Vol. 329, No. 25, pp.5249–5272.

Yoon, J. and Singh, R.Y. (2010b) 'Dynamic force transmitted by hydraulic mount: estimation in frequency domain using motion and/or pressure measurements and quasi-linear models', *Noise. Control. Eng. J.*, Vol. 58, No. 4, pp.403–419.

Yu, Y., Naganathan, N.G. and Dukkipati, R.V. (2001a) 'A literature review of automotive car engine mounting systems', *Mech. Mach. Theory.*, Vol. 36, No. 1, pp.123–142.

Yu, Y., Peelamedu, S.M., Naganathan, N.G. and Dukkipati, R.V. (2001b) 'Automotive car engine mounting systems: a survey', *J. Dyn. Syst.-T.*, Vol. 123, No. 2, pp.186–194, ASME.